

A Stable FE Method For the Space-Time Solution of the Cahn-Hilliard Equation

Eirik Valseth^{a,*}, Albert Romkes^b, Austin R. Kaul^b

^aOden Institute for Computational Engineering and Sciences, The University of Texas at Austin, Austin, TX 78712, USA

^bDepartment of Mechanical Engineering, South Dakota School of Mines & Technology, Rapid City, SD 57701, USA

ARTICLE INFO

Article history:

Cahn-Hilliard equation, phase field transition, discontinuous Petrov-Galerkin and Adaptivity
2000 MSC: 65M60 65N12 35G61

ABSTRACT

In its application to the modeling of a mineral separation process, we propose the numerical analysis of the Cahn-Hilliard equation by employing space-time discretizations of the automatic variationally stable finite element (AVS-FE) method. The AVS-FE method is a Petrov-Galerkin method which employs the concept of optimal discontinuous test functions of the discontinuous Petrov-Galerkin (DPG) method by Demkowicz and Gopalakrishnan. The trial space, however, consists of globally continuous Hilbert spaces such as $H^1(\Omega)$ and $H(\text{div}, \Omega)$. Hence, the AVS-FE approximations employ classical C^0 or Raviart-Thomas FE basis functions. The optimal test functions guarantee the numerical stability of the AVS-FE method and lead to discrete systems that are symmetric and positive definite. Hence, the AVS-FE method can solve the Cahn-Hilliard equation in both space and time without a restrictive CFL condition to dictate the space-time element size. We present numerical verifications of both one and two dimensional problems in space. The verifications show optimal rates of convergence in $L^2(\Omega)$ and $H^1(\Omega)$ norms. Results for mesh adaptive refinements using a built-in error estimator of the AVS-FE method are also presented.

© 2025 Elsevier Inc. All rights reserved.

1. Introduction

The refinement and concentration of minerals from mineral ores is a process that typically requires the use of water such as flowing film and froth flotation concentrators. Processing facilities in the United States consume large amounts of water, in some cases up to $60,000m^3$ each day [1]. Therefore, sustainable approaches to mineral concentration

*This work has been supported by the NSF CBET Program, under NSF Grant titled *Sustainable System for Mineral Beneficiation*, NSF Grant No. 1805550.

*Corresponding author

e-mail: Eirik@utexas.edu (Eirik Valseth), Albert.Romkes@sdsmt.edu (Albert Romkes), Austin.Kaul@mines.sdsmt.edu (Austin R. Kaul)

that significantly reduce or remove the need for water are needed to aid in conservation efforts. Furthermore, the location of several copper mines in the United States are in arid regions of the Southwest, thereby further increasing the importance of conservation efforts. It has been proposed by researchers at South Dakota School of Mines & Technology (SDSM&T) to exploit the adhesion forces between mineral particles and specifically tailored substrates to develop new mineral separation techniques using as little water as possible. Thus, a new type of mineral separator must be developed and designed. To aid in the design process, it is necessary to predict the mineral separation process which requires simulation of the accumulation of mineral particles on chemically treated substrates. This accumulation is to be modeled by the Cahn-Hilliard equation.

The mathematical analysis and well posedness results for the Cahn-Hilliard equation have been established in, e.g., [2] by Bowey and Elliott, thereby setting the stage for the application of a FE method in its approximation. However, there are two challenges: *i*) the nonlinearity of the Cahn-Hilliard equation and *ii*) the transient nature of this problem leading to a loss of the numerical stability for the classical FE method. The second challenge is typically critical, as FE methods for nonlinear problems have been established successfully in, e.g., [3]. To achieve stability in the classical FE method, the FE mesh partition, i.e., element size, must be fine enough to establish numerically stable FE approximations thereby leaving classical FE methods not the most suitable for the approximation of the Cahn-Hilliard equation. Classically, when solving transient partial differential equations (PDE)s in a FE framework, a method of lines approach is taken, i.e., FE methods are employed in the spatial domain whereas the temporal domain is discretized by a finite difference scheme. The numerical stability of finite difference schemes are then established through the Courant-Friedrichs-Lewy (CFL) condition [4]. This classical approach has been employed by several authors to establish approximations of the Cahn-Hilliard equation using several flavors of FE methods including least squares FE method, discontinuous Galerkin methods, and isogeometric analysis (see [5–11]).

An alternative to temporal discretizations using difference methods and a CFL condition are conditionally stable FE methods which have been successfully applied to transient problems, see, e.g., [12–14]. While these space-time methods have been successful in the FE approximation of transient phenomena, their conditional stability requires arduous *a priori* analyses to properly determine their stabilization parameters. Unconditionally stable FE methods are also applicable for transient PDEs such as the DPG method [15–17] or least squares FE methods [18]. Fernandino and Dorao [10] applied the least squares FE method successfully to a Cahn-Hilliard problem in both space and time using basis functions that are of higher order continuity than classical FE methods. The computational cost of these space-time FE methods are typically higher than the method of lines approach but the FE formulations can employ a wide range of tools such as *a priori* and *a posteriori* error estimation and *hp*–adaptive refinement strategies in both space and time. Thus, the (potential) additional computational cost can be justified.

The AVS-FE method, introduced by Calo, Romkes, and Valseth in [19], is an unconditionally stable FE method, i.e., the AVS-FE approximations are guaranteed to remain stable for any PDE as long as the kernel of the underlying differential operator is trivial [20]. This method is a Petrov-Galerkin method in which the trial space consist of globally continuous classical FE basis and the test space of piecewise discontinuous functions. Hence, it is a hybrid between the DPG method of Demkowicz and Gopalakrishnan [21] and classical FE methods. In addition to its unconditional

stability, other features of the AVS-FE method are highly accurate flux approximations, due to its first-order system setting, and its ability to compute optimal discontinuous test functions on the fly, element-by-element.

In this paper, we develop space-time AVS-FE approximations of the Cahn-Hilliard equation. A space-time AVS-FE method is chosen to exploit its unconditional stability property, its convergence properties, and the built-in error indicators allowing us to employ mesh adaptive refinement strategies. The Cahn-Hilliard equation being nonlinear requires special treatment and we take the approach of Carstensen *et al.* in [22]. To start, we introduce the mineral processing application and the corresponding model Cahn-Hilliard boundary value problem (BVP), in addition to notations and conventions in Section 2. Next, we review the AVS-FE methodology in Section 2.2 for linear problems and introduce the concepts of [22] to be employed to perform nonlinear iterations. In Section 3, we derive the equivalent AVS-FE weak formulation for the Cahn-Hilliard BVP. In Section 4, we perform multiple numerical verifications. First, in Section 4.1, we present a verification for a spatially one dimensional problem possessing an exact solution resulting in numerical evidence of optimal rates of convergence, as well as a verification of a space-time adaptive mesh refinement. Then, in Section 4.2, we present a classical phase separation problem for the Cahn-Hilliard problem from literature that is spatially two dimensional. Finally, we conclude with remarks on the results and future works in Section 5.

2. Model Problem and Review of the AVS-FE Method

2.1. Model Problem

The Cahn-Hilliard equation [23] was introduced to model the evolution of the phase transition of components in a binary alloy from a mixed to a separated state. The equation is a fourth order nonlinear PDE and can be found in several forms in literature. Here, we consider the following form:

$$-\frac{\partial u}{\partial t} + D\Delta[u^3 - u - \lambda\Delta u] = 0, \quad (1)$$

where Δ denotes the spatial Laplacian, $D \in L^\infty(\Omega)$ is the diffusion coefficient, and $\lambda \in L^\infty(\Omega)$ is the square of the width of the transition region in the separation process. Note that D is of unit $\frac{m^2}{s}$ and $\sqrt{\lambda}$ is of unit m^2 .

In collaboration with a team of metallurgists at the SDSM&T, we propose to use the Cahn-Hilliard equation to model a particular mineral separation process. The proposed mineral separation process will exploit the forces of adhesion between mineral particles and substrates, both of which are potentially treated, i.e., functionalized to ensure maximum adhesion of desirable minerals. In Figure 1, a conceptual sketch of the process is shown. Ore enters the separator in a stream of air, where the desirable minerals adhere to the substrate and the remainder of the ore ends up in what is referred to as tailings. The motivation for the development of this type of separation process stems from the fact that it would greatly reduce the use of water compared to currently used techniques. These generally consist of flotation processes which require large amounts of water to establish proper mineral separation from the ore. Now, in the design of the newly proposed separation method, it is necessary to predict the separation of the mineral concentration as it accumulates onto the substrate. To do so, we propose to use the Cahn-Hilliard equation.

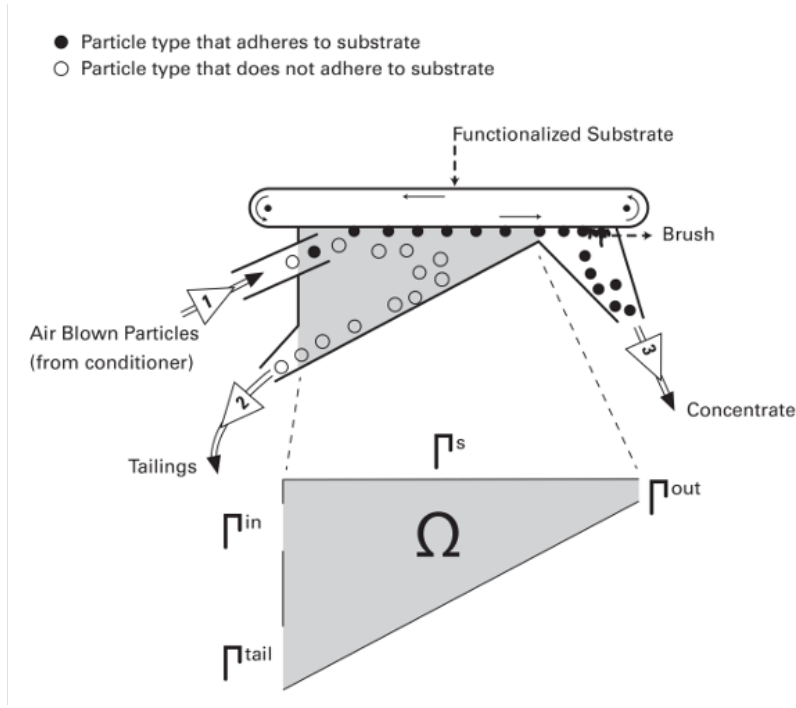


Fig. 1. Conceptual sketch of mineral separator (Courtesy of Brian Hill of University Relations at SDSM&T).

In the particular application of the Cahn-Hilliard equation to the mineral separation process, the concentration function $u = u(\mathbf{x}, t)$ represents the mineral concentration at a material point \mathbf{x} and time t . Thus, in the spirit of the original application of this equation, a value $u(\mathbf{x}, t) = 1$ represents the scenario in which the desired mineral has separated from the flow of minerals and has adhered to the substrate. Conversely, a value $u(\mathbf{x}, t) = 0$ denotes the scenario in which the desired mineral particle is still fully dispersed in the flow of minerals. Values between 0 and 1 identify areas in which the mineral particles are in the process of separating.

For the mathematical model of the separation process, we consider only the portion of the mineral separator in which the mineral separation occurs. The boundary, which encloses the separator is assumed to consist of several disjoint portions corresponding to the substrate (onto which the mineral accumulates), the inflow boundary (where the minerals enter the separator), the tailing boundary (where minerals that fail to adhere to the substrate exit the separator), and finally the outflow boundary (where the accumulated minerals exit the separator). Additionally, there may be additional portions of the boundary that serve to encompass the separation process. In Figure 1, an example mineral separator computational domain Ω is shown.

To establish approximations of the Cahn-Hilliard equation, proper boundary and initial conditions are needed to guarantee physically meaningful results. Let $\Omega \subset \mathbb{R}^2$ be an open bounded domain (see Figure 1) with Lipschitz boundary $\partial\Omega$ and outward unit normal vector \mathbf{n} . Also, let $t = 0$ be the initial time and $t = T$ the final time. The boundary $\partial\Omega$ consists of open subsections:

- Γ_s - the portion of $\partial\Omega$ that coincides with the functionalized substrate upon which mineral accumulation occurs.

- Γ_{in} - the inflow boundary.
- Γ_{out} - the portion of the boundary $\partial\Omega$ through which the accumulated separated mineral exits the separator.
- Γ_{tail} - the outflow boundary, containing the mineral particles that failed to adhere.
- Γ_0 - the remaining portion of the boundary $\partial\Omega$ which contains the entire separation process.

The intersection of these portions is empty and $\partial\Omega = \overline{\Gamma_s \cup \Gamma_{in} \cup \Gamma_{out} \cup \Gamma_{tail} \cup \Gamma_0}$. With the boundary identified by these subsets, the proper boundary conditions for the case of mineral separation are as follows:

- $u = 1, \mathbf{x} \in \Gamma_s, t \in [0, T]$, i.e., the mineral particles have adhered to the substrate and separated from the flow field .
- $u = 0, \mathbf{x} \in \partial\Omega \setminus \Gamma_s, t \in [0, T]$, i.e., no mineral particles adhere to the remainder of the separator.
- $u^3 - u - \lambda \Delta u = 0, \mathbf{x} \in \partial\Omega, t \in [0, T]$, if there is no separation ongoing, the "chemical potential" $u^3 - u - \lambda \Delta u$ must vanish .

Finally, the initial conditions for the mineral separation application are:

- $u = u_{in}, \mathbf{x} \in \Gamma_{in}, t = 0$, i.e., we assume the separator has no material in it at the onset of the separation process. Hence, the initial conditions are zero on all boundaries.
- $u = 0, \mathbf{x} \in \partial\Omega \setminus \Gamma_s, t = 0$.
- $u = 0, \mathbf{x} \in \Omega, t = 0$.
- $u^3 - u - \lambda \Delta u = 0, \mathbf{x} \in \Omega, t = 0$.

where u_{in} is the concentration of the desired mineral as it enters the separator.

With boundary and initial conditions defined along with the PDE (1), we consider the following Cahn-Hilliard initial boundary value problem (IBVP):

Find u such that:

$$\begin{aligned} -\frac{\partial u}{\partial t} + D\Delta[u^3 - u - \lambda \Delta u] &= 0, & \text{in } \Omega \times [0, T], \\ u &= u_0, & \text{on } \partial\Omega, \\ u &= u_{initial}, & \text{on } t = 0 \cap \partial\Omega, \\ u^3 - u - \lambda \Delta u &= g, & \text{on } \partial\Omega, \end{aligned} \tag{2}$$

where the values of u_0 , $u_{initial}$, and g are as given in the preceding lists. For generality, we keep these arbitrary and employ specific choices in the numerical verifications of Section 4.

While the goal of the current research project is to use the Cahn-Hilliard equation as a model problem for mineral separation and the design of a mineral separator, we limit our presentation to the numerical approximation of the Cahn-Hilliard initial boundary value problem (IBVP) on general domains Ω as this is a key stepping stone towards the research goal and the design of the separator is still work in progress.

2.2. Review of the AVS-FE method

The AVS-FE method has been introduced by Calo, Romkes and Valseth in [19]. Attractive features of the AVS-FE method are its unconditional numerical stability property, regardless whether the underlying differential operator is self-adjoint or not, and its highly accurate flux approximations. The AVS-FE method is a Petrov-Galerkin method in which the trial space consist of classical piecewise continuous FE basis functions, and the test space consist of piecewise discontinuous functions. The discontinuous test space is spanned by so called 'optimal' test functions that are computed on-the-fly by invoking the DPG philosophy [21, 24–28].

To introduce the AVS-FE method here, we consider a domain Ω partitioned into elements:

$$\Omega = \text{int}\left(\bigcup_{K_m \in \mathcal{P}_h} \overline{K_m}\right), \quad (3)$$

and abstract AVS-FE weak form in which the underlying differential operator is linear:

Find $\mathfrak{u} \in U(\Omega)$ such that:

$$B(\mathfrak{u}; \mathfrak{v}) = F(\mathfrak{v}), \quad \forall \mathfrak{v} \in V(\mathcal{P}_h),$$

(4)

where \mathfrak{u} and \mathfrak{v} are the vector valued trial and test functions, respectively, $U(\Omega)$ is the trial space, $V(\mathcal{P}_h)$ the broken test space, $B : U(\Omega) \times V(\mathcal{P}_h) \rightarrow \mathbb{R}$ is the bilinear form, $F : V(\mathcal{P}_h) \rightarrow \mathbb{R}$ the linear 'load' functional, and \mathcal{P}_h denotes the partition of Ω into finite elements (see (3)). In the AVS-FE method, $U(\Omega)$ is a globally continuous Hilbert space as used in classical FE methods. However, $V(\mathcal{P}_h)$ is a broken space consisting of functions that are globally in $L^2(\Omega)$ and locally may be of higher order (e.g., $H^1(K_m)$). The kernel of $B(\cdot; \cdot)$ is assumed to be trivial to guarantee the uniqueness of solutions (as in any other FE method).

With the assumption on the kernel of the bilinear form in place, the AVS-FE method introduces the following *energy norm* $\|\cdot\|_B : U(\Omega) \rightarrow [0, \infty)$:

$$\|\mathfrak{u}\|_B \stackrel{\text{def}}{=} \sup_{\mathfrak{v} \in V(\mathcal{P}_h) \setminus \{0\}} \frac{|B(\mathfrak{u}; \mathfrak{v})|}{\|\mathfrak{v}\|_{V(\mathcal{P}_h)}}. \quad (5)$$

The well posedness of the AVS-FE weak formulation is then established by the following lemma:

Lemma 2.1 *Let the source and Neumann data be sufficiently regular. Then, the weak formulation (4) is well posed and has a unique solution.*

Proof: The proof follows from the Generalized Lax-Milgram Theorem, as $B(\cdot, \cdot)$ satisfies the Inf-sup condition as well as the continuity condition in terms of the energy norm (5), (see [20] or [21, 27] for details). □

By deriving the weak statement such that the trial spaces are global Hilbert spaces, the AVS-FE method seeks FE approximations \mathfrak{u}^h of \mathfrak{u} of (4) in which the trial functions in the discretization are classical FE basis functions that span the FE trial space $U^h(\Omega)$, e.g., $H^1(\Omega)$ or $H(\text{div}, \Omega)$. Hence, we represent the approximations of the components $\mathfrak{u}^h(\mathbf{x})$ as linear combinations of trial functions $e^i(\mathbf{x}) \in U^h(\Omega)$ and the corresponding degrees of freedom, \mathfrak{u}_i^h . Conversely, to construct the test space $V^*(\mathcal{P}_h)$ we compute piecewise discontinuous *optimal* test functions that guarantee

unconditionally stable discretizations. These optimal test functions are obtained by employing the DPG philosophy [21, 24–28] in which *global* optimal test functions are established through *global* weak problems. However, even though the optimal test functions are global functions, they have compact support and, in the case of the AVS-FE method their support is identical to that of the trial functions. Additionally, the local restrictions are computed in a completely decoupled fashion, i.e., element-by-element, with high accuracy (see [19] for details). Thus, e.g., for the local restriction of a trial function \mathfrak{e}^i on an element $K_m \in \mathcal{P}_h$, i.e., a shape function, we solve the corresponding optimal test function $\hat{\mathfrak{e}}^i(\mathbf{x})$ from the following *local* problem on K_m :

$$(\mathfrak{T}; \hat{\mathfrak{e}}^i)_{V(K_m)} = B|_{K_m}(\mathfrak{e}^i; \mathfrak{T}), \quad \forall \mathfrak{T} \in V(K_m), \quad (6)$$

where $B|_{K_m}(\cdot; \cdot)$ denotes the restriction of $B(\cdot; \cdot)$ to the element K_m , $V(K_m)$ the local restriction of the test space to K_m , and $(\cdot; \cdot)_{V(K_m)} : V(K_m) \times V(K_m) \rightarrow \mathbb{R}$, is a local inner product on $V(K_m)$. see [19] for details.

Finally, we introduce the FE discretization of (4) governing the approximation $\mathfrak{u}^h \in U^h(\Omega)$ of \mathfrak{u} :

Find $\mathfrak{u}^h \in U^h(\Omega)$ such that:

$$B(\mathfrak{u}^h; \mathfrak{v}^h) = F(\mathfrak{v}^h), \quad \forall \mathfrak{v}^h \in V^*(\mathcal{P}_h),$$

(7)

where the finite dimensional subspace of test functions $V^*(\mathcal{P}_h) \subset V(\mathcal{P}_h)$ is spanned by the optimal test functions.

By using the DPG philosophy to construct $V^*(\mathcal{P}_h)$, the discrete problem (7) inherits the continuity and inf-sup constants of the continuous problem (see, e.g., [20] for the proof). Hence, the AVS-FE discretization is unconditionally stable for any choice of element size h_m and local degree of polynomial approximation p_m . A further consequence of the optimal test functions is that the global stiffness matrix is symmetric and positive definite regardless of the character of the underlying differential operator (self adjoint or non-self adjoint).

Remark 2.1 *Instead of computing the optimal test functions from (6) on-the-fly to construct the FE system of linear algebraic equations, one can consider another, alternative, interpretation of the AVS-FE method. This alternative interpretation is in the DPG literature [29–31] referred to as a mixed or saddle point problem and is a result of the fact that DPG and AVS-FE methods are constrained minimization techniques:.*

Find $\mathfrak{u}^h \in U^h(\Omega)$, $\hat{\mathfrak{E}}^h \in V^*(\mathcal{P}_h)$ such that:

$$\begin{aligned} (\hat{\mathfrak{E}}^h, \mathfrak{v}^h)_{V(\mathcal{P}_h)} - B(\mathfrak{u}^h, \mathfrak{v}^h) &= -F(\mathfrak{v}^h), \quad \forall \mathfrak{v}^h \in V^*(\mathcal{P}_h), \\ B(\mathfrak{p}^h, \hat{\mathfrak{E}}^h) &= 0, \quad \forall \mathfrak{p}^h \in U^h(\Omega). \end{aligned}$$

(8)

The second equation of (8) represents the constraint in which the Gateaux derivative of the bilinear form is acting on the approximate "error representation" function $\hat{\mathfrak{E}}^h$. This function is a Riesz representer of the approximation error $\mathfrak{u} - \mathfrak{u}^h$ and leads to an identity between the energy norm of the approximation error and the norm of the error representation function on $V(\mathcal{P}_h)$. Hence, the norm $\|\hat{\mathfrak{E}}\|_{V(\mathcal{P}_h)}$ is an a posteriori error estimate and its local restriction may be employed as an error indicator in mesh adaptive strategies. For details on these error indicators and the derivation of the mixed formulation, see [20] or [29]. Note that since we, at this point, have assumed that the underlying differential operator is linear, the Gateaux derivative of the bilinear form is identical to itself.

This mixed form allows straightforward implementation in high level FE solvers such as Firedrake [32] and FEniCS [33]. The cost of solving the resulting system of linear algebraic equations from (8) is larger than the 'classical' AVS-FE method since now the optimal test functions are essentially computed by solving global problems. However, it has the clear advantage for hp-adaptive strategies, since upon solving (8), it immediately provides a posteriori error estimators and error indicators that can drive the mesh adaptive process.

3. AVS-FE Weak Formulation and Discretization of The Cahn-Hilliard Equation

With the notations introduced in Section 2 and the review of the AVS-FE method above, we proceed to derive the AVS-FE weak formulation for the Cahn-Hilliard IBVP. To this end, let us consider the following general form of the Cahn-Hilliard IBVP (2):

Find u such that:

$$\begin{aligned} -\frac{\partial u}{\partial t} + D \Delta [u^3 - u - \lambda \Delta u] &= 0, & \text{in } \Omega_T, \\ u &= u_0, & \text{on } \partial\Omega_T, \\ u^3 - u - \lambda \Delta u &= g, & \text{on } \partial\Omega_T, \end{aligned} \quad (9)$$

where $\Omega_T = \Omega \times [0, T]$ is the space-time domain, $D \in L^\infty(\Omega)$, and $\lambda \in L^\infty(\Omega)$. The diffusion coefficient D and the square width of the transition region λ are considered to be constant throughout the domain. To derive the weak formulation, we use a regular partition \mathcal{P}_T^h of Ω_T into elements K_m , such that:

$$\Omega_T = \text{int}\left(\bigcup_{K_m \in \mathcal{P}_T^h} \overline{K_m}\right). \quad (10)$$

We apply a mixed FE methodology and introduce two flux variables \mathbf{r}, \mathbf{t} and an additional scalar variable q as auxiliary variables:

- $\mathbf{r} = \{r_x, r_y\}^T = \nabla u$.
- $q = u^3 - u - \lambda \nabla \cdot \mathbf{r}$.
- $\mathbf{t} = \{t_x, t_y\}^T = \nabla q$.

Where ∇ denotes the spatial gradient operator. Note that this definition of the flux variables means that they do not explicitly depend on time. Hence, this dictates that the regularity of these trial functions are $\mathbf{r} \in H(\text{div}, \Omega)$, $\mathbf{t} \in H(\text{div}, \Omega)$, $q \in H^1(\Omega_T)$, $u \in H^1(\Omega_T)$, and the IBVP (9) can be recast as an equivalent first-order system of PDEs:

Find $(u, q, \mathbf{r}, \mathbf{t}) \in H^1(\Omega_T) \times H^1(\Omega_T) \times H(\text{div}, \Omega) \times H(\text{div}, \Omega)$ such that:

$$\begin{aligned} \nabla u - \mathbf{r} &= \mathbf{0}, & \text{in } \Omega, \\ \nabla q - \mathbf{t} &= \mathbf{0}, & \text{in } \Omega, \\ u^3 - u - \lambda \nabla \cdot \mathbf{r} - q &= 0, & \text{in } \Omega_T, \\ -\frac{\partial u}{\partial t} + D \nabla \cdot \mathbf{t} &= 0, & \text{in } \Omega_T, \\ u &= u_0, & \text{on } \partial\Omega_T, \\ q &= g, & \text{on } \partial\Omega_T. \end{aligned} \quad (11)$$

We proceed to enforce the PDEs (11) weakly on each element $K_m \in \mathcal{P}_T^h$ and sum the contributions from all $K_m \in \mathcal{P}_T^h$, i.e.,

$$\begin{aligned} & \text{Find } (u, q, \mathbf{r}, \mathbf{t}) \in H^1(\Omega_T) \times H^1(\Omega_T) \times H(\text{div}, \Omega) \times H(\text{div}, \Omega) : \\ & \sum_{K_m \in \mathcal{P}_h} \int_{K_m} \left\{ [\nabla u - \mathbf{r}] \cdot \mathbf{s}_m + [\nabla q - \mathbf{t}] \cdot \mathbf{p}_m + [u^3 - u - \lambda \nabla \cdot \mathbf{r} - q] v_m \right. \\ & \quad \left. + \left[-\frac{\partial u}{\partial t} + D \nabla \cdot \mathbf{t} \right] w_m \right\} d\mathbf{x} = 0, \\ & \forall (v_m, w_m, \mathbf{s}_m, \mathbf{p}_m) \in L^2(\Omega) \times L^2(\Omega) \times [L^2(\Omega)]^2 \times [L^2(\Omega)]^2. \end{aligned} \quad (12)$$

Next, we apply Green's identity to the terms multiplied with the scalar valued test functions v_m and w_m which dictates that we increase the regularity of each scalar valued test function to be in H^1 locally for every $K_m \in \mathcal{P}_h$, i.e.,

$$\begin{aligned} & \text{Find } (u, q, \mathbf{r}, \mathbf{t}) \in H^1(\Omega_T) \times H^1(\Omega_T) \times H(\text{div}, \Omega) \times H(\text{div}, \Omega) : \\ & \sum_{K_m \in \mathcal{P}_h} \left\{ \int_{K_m} \left[[\nabla u - \mathbf{r}] \cdot \mathbf{s}_m + [\nabla q - \mathbf{t}] \cdot \mathbf{p}_m + [u^3 - u - q] v_m \right. \right. \\ & \quad \left. \left. + \lambda \mathbf{r} \cdot \nabla v_m - \frac{\partial u}{\partial t} w_m - D \mathbf{t} \cdot \nabla w_m \right] d\mathbf{x} \right. \\ & \quad \left. + \oint_{\partial K_m} D \gamma_{\mathbf{n}}^m(\mathbf{t}) \gamma_0^m(w_m) - \lambda \gamma_{\mathbf{n}}^m(\mathbf{r}) \gamma_0^m(v_m) ds \right\} = 0, \\ & \forall (v_m, w_m, \mathbf{s}_m, \mathbf{p}_m) \in H^1(\mathcal{P}_T^h) \times H^1(\mathcal{P}_T^h) \times [L^2(\Omega)]^2 \times [L^2(\Omega)]^2, \end{aligned} \quad (13)$$

where the broken H^1 space on the partition \mathcal{P}_T^h is defined:

$$H^1(\mathcal{P}_T^h) \stackrel{\text{def}}{=} \left\{ v \in L^2(\Omega_T) : v_m \in H^1(K_m), \forall K_m \in \mathcal{P}_T^h \right\}. \quad (14)$$

The operators $\gamma_0^m : H^1(K_m) \rightarrow H^{1/2}(\partial K_m)$ and $\gamma_{\mathbf{n}}^m : H(\text{div}, K_m) \rightarrow H^{-1/2}(\partial K_m)$ denote the trace and normal trace operators (e.g., see [34]) on K_m ; and \mathbf{n}_m is the outward unit normal vector to the element boundary ∂K_m of K_m . Note that the edge integrals on ∂K_m are to be interpreted as the duality pairings $\langle \cdot, \cdot \rangle_{H^{-1/2}(\partial K_m) \times H^{1/2}(\partial K_m)}$. Instead, we use an integral representation here, as is engineering convention.

Note that the edge integrals in (13) only concern the auxiliary flux unknowns \mathbf{r} and \mathbf{t} . Thus, any Dirichlet boundary conditions on u and q must be enforced strongly. Alternatively, we could perform further applications of Green's identity to shift all the derivatives to the test functions, which would allow the weak enforcement of both BCs in (11). Finally, these boundary conditions are incorporated in the space $U(\Omega_T)$ and we arrive at the AVS-FE weak statement for the Cahn-Hilliard IBVP:

$$\begin{aligned} & \text{Find } (u, q, \mathbf{r}, \mathbf{t}) \in U(\Omega_T) : \\ & \sum_{K_m \in \mathcal{P}_h} \left\{ \int_{K_m} \left[[\nabla u - \mathbf{r}] \cdot \mathbf{s}_m + [\nabla q - \mathbf{t}] \cdot \mathbf{p}_m + [u^3 - u - q] v_m \right. \right. \\ & \quad \left. \left. + \lambda \mathbf{r} \cdot \nabla v_m - \frac{\partial u}{\partial t} w_m - D \mathbf{t} \cdot \nabla w_m \right] d\mathbf{x} \right. \\ & \quad \left. + \oint_{\partial K_m} D \gamma_{\mathbf{n}}^m(\mathbf{t}) \gamma_0^m(w_m) - \lambda \gamma_{\mathbf{n}}^m(\mathbf{r}) \gamma_0^m(v_m) ds \right\} = 0, \\ & \forall (v_m, w_m, \mathbf{s}_m, \mathbf{p}_m) \in V(\mathcal{P}_T^h), \end{aligned} \quad (15)$$

where the trial and test spaces $U(\Omega_T)$ and $V(\mathcal{P}_T^h)$ are defined:

$$\begin{aligned} U(\Omega_T) &\stackrel{\text{def}}{=} \left\{ (u, q, \mathbf{r}, \mathbf{t}) \in H^1(\Omega_T) \times H^1(\Omega_T) \times H(\text{div}, \Omega) \times H(\text{div}, \Omega) : \right. \\ &\quad \left. \gamma_0^m(u)|_{\partial K_m \cap \partial \Omega_T} = u_0, \gamma_0^m(q)|_{\partial K_m \cap \partial \Omega_T} = g, \forall K_m \in \mathcal{P}_T^h \right\}, \\ V(\mathcal{P}_T^h) &\stackrel{\text{def}}{=} H^1(\mathcal{P}_T^h) \times H^1(\mathcal{P}_T^h) \times [L^2(\Omega)]^2 \times [L^2(\Omega)]^2, \end{aligned} \quad (16)$$

with norms $\|\cdot\|_{U(\Omega_T)} : U(\Omega_T) \rightarrow [0, \infty)$ and $\|\cdot\|_{V(\mathcal{P}_T^h)} : V(\mathcal{P}_T^h) \rightarrow [0, \infty)$ defined as:

$$\begin{aligned} \|(u, q, \mathbf{r}, \mathbf{t})\|_{U(\Omega_T)} &\stackrel{\text{def}}{=} \sqrt{\int_{\Omega} \left[(u, u)_{H^1(\Omega)} + (q, q)_{H^1(\Omega)} + (\mathbf{r}, \mathbf{r})_{H(\text{div}, \Omega)} + (\mathbf{t}, \mathbf{t})_{H(\text{div}, \Omega)} \right] \mathbf{d}\mathbf{x}}, \\ \|(v, w, \mathbf{s}, \mathbf{p})\|_{V(\mathcal{P}_T^h)} &\stackrel{\text{def}}{=} \sqrt{\sum_{K_m \in \mathcal{P}_T^h} \int_{K_m} \left[h_m^2 \nabla v_m \cdot \nabla v_m + v_m^2 + h_m^2 \nabla w_m \cdot \nabla w_m + w_m^2 + \mathbf{s}_m \cdot \mathbf{s}_m + \mathbf{p}_m \cdot \mathbf{p}_m \right] \mathbf{d}\mathbf{x}}. \end{aligned} \quad (17)$$

By introducing the sesquilinear form $B : U(\Omega_T) \times V(\mathcal{P}_T^h) \rightarrow \mathbb{R}$:

$$\begin{aligned} B((u, q, \mathbf{r}, \mathbf{t}); (v, w, \mathbf{s}, \mathbf{p})) &\stackrel{\text{def}}{=} \sum_{K_m \in \mathcal{P}_h} \left\{ \int_{K_m} \left[[\nabla u - \mathbf{r}] \cdot \mathbf{s}_m + [\nabla q - \mathbf{t}] \cdot \mathbf{p}_m + [u^3 - u - q] v_m \right. \right. \\ &\quad \left. \left. + \lambda \mathbf{r} \cdot \nabla v_m - \frac{\partial u}{\partial t} w_m - D \mathbf{t} \cdot \nabla w_m \right] \mathbf{d}\mathbf{x} \right. \\ &\quad \left. + \oint_{\partial K_m} D \gamma_{\mathbf{n}}^m(\mathbf{t}) \gamma_0^m(w_m) - \lambda \gamma_{\mathbf{n}}^m(\mathbf{r}) \gamma_0^m(v_m) \mathbf{d}\mathbf{s} \right\}, \end{aligned} \quad (18)$$

we can write the weak formulation (15) compactly:

Find $(u, q, \mathbf{r}, \mathbf{t}) \in U(\Omega_T)$ such that:

$$B((u, q, \mathbf{r}, \mathbf{t}); (v, w, \mathbf{s}, \mathbf{p})) = 0, \quad \forall (v, w, \mathbf{s}, \mathbf{p}) \in V(\mathcal{P}_T^h).$$

(19)

3.1. AVS-FE Discretizations

We seek numerical approximations $(u^h, q^h, \mathbf{r}^h, \mathbf{t}^h)$ of $(u, q, \mathbf{r}, \mathbf{t})$ by using classical FE trial basis functions such as Lagrange interpolants or Raviart-Thomas polynomials. However, the test space is discretized by employing the DPG philosophy and we use optimal test functions as computed from the discrete Riesz problems (see (4)). Thus, the FE discretization of (19) governing $(u^h, q^h, \mathbf{r}^h, \mathbf{t}^h) \in U^h(\Omega_T)$ is:

Find $(u^h, q^h, \mathbf{r}^h, \mathbf{t}^h) \in U^h(\Omega_T)$ such that:

$$B((u^h, q^h, \mathbf{r}^h, \mathbf{t}^h); (v^h, w^h, \mathbf{s}^h, \mathbf{p}^h)) = 0, \quad \forall (v^h, w^h, \mathbf{s}^h, \mathbf{p}^h) \in V^*(\mathcal{P}_T^h),$$

(20)

where the finite dimensional test space $V^*(\mathcal{P}_T^h) \subset V(\mathcal{P}_T^h)$ is spanned by numerical approximations of the test functions through the Riesz representation problems, analogous to (6).

Note that all the trial variables $(u^h, q^h, \mathbf{r}^h, \mathbf{t}^h)$ are time dependent (either directly or indirectly). By exploiting the unconditional discrete stability of the AVS-FE method, the entire space-time domain is discretized by finite elements instead of using traditional time stepping techniques satisfying a CFL condition. Hence, we have significant flexibility in the choice of mesh parameters in the FE discretization.

To solve the nonlinear variational problem, we can linearize the weak form and solve a sequence of linear discrete problems that converge to the nonlinear solution. This can be achieved by employing solution procedures such as Newton iterations to (20) to which we compute on-the-fly optimal test functions at each step of the Newton iterations. However, we consider an equivalent mixed or saddle point problem interpretation of the AVS-FE, as introduced in Section 2.2, in which we seek both $(u^h, q^h, \mathbf{r}^h, \mathbf{t}^h)$ and the error representation function $(\psi^h, \varphi^h, \xi^h, \eta^h)$:

$$\begin{aligned} & \text{Find } (u^h, q^h, \mathbf{r}^h, \mathbf{t}^h) \in U^h(\Omega_T), (\psi^h, \varphi^h, \xi^h, \eta^h) \in V^*(\mathcal{P}_T^h) \text{ such that:} \\ & ((\psi^h, \varphi^h, \xi^h, \eta^h), (v^h, w^h, \mathbf{s}^h, \mathbf{p}^h))_{V(\mathcal{P}_T^h)} - B((u^h, q^h, \mathbf{r}^h, \mathbf{t}^h); (v^h, w^h, \mathbf{s}^h, \mathbf{p}^h)) = 0, \\ & \quad \quad \quad \forall (v^h, w^h, \mathbf{s}^h, \mathbf{p}^h) \in V^*(\mathcal{P}_T^h), \\ & B'_{\mathfrak{u}}((a^h, b^h, \mathbf{c}^h, \mathbf{d}^h); (\psi^h, \varphi^h, \xi^h, \eta^h)) = 0, \\ & \quad \quad \quad \forall ((a^h, b^h, \mathbf{c}^h, \mathbf{d}^h)) \in U^h(\Omega_T). \end{aligned} \tag{21}$$

Where the operator $B'_{\mathfrak{u}} : U(\Omega_T) \times V(\mathcal{P}_T^h) \longrightarrow \mathbb{R}$ is the first order Gateaux derivative of the sesquilinear form B with respect to $\mathfrak{u} = (u, q, \mathbf{r}, \mathbf{t})$. Application of the definition of the Gateaux derivative then gives:

$$\begin{aligned} B'_{\mathfrak{u}}((a, b, \mathbf{c}, \mathbf{d}); (\psi, \varphi, \xi, \eta)) & \stackrel{\text{def}}{=} \sum_{K_m \in \mathcal{P}_T^h} \left\{ \int_{K_m} \left[[\nabla a - \mathbf{c}] \cdot \xi_m + [\nabla b - \mathbf{d}] \cdot \eta_m \right. \right. \\ & \quad \left. \left. + [3u^2 a - a - b] \psi_m + \beta \mathbf{c} \cdot \nabla \psi_m - \frac{\partial a}{\partial t} \varphi_m - D \mathbf{d} \cdot \nabla \varphi_m \right] \mathrm{d} \mathbf{x} \right. \\ & \quad \left. + \oint_{\partial K_m} D \gamma_{\mathbf{n}}^m(\mathbf{d}) \gamma_0^m(\varphi_m) - \beta \gamma_{\mathbf{n}}^m(\mathbf{c}) \gamma_0^m(\psi_m) \mathrm{d} s \right\} \end{aligned} \tag{22}$$

4. Numerical Verifications

In this section, we present several numerical verifications applying the AVS-FE method to (spatially) one and two dimensional problems. The presented verifications are commonly used benchmark problems for the Cahn-Hilliard BVP that allow us to compare our results to those in existing literature. To establish the solution of (21) we use the high level FE solvers Firedrake [32] and FEniCS [33] which in turn employ the Portable, Extensible Toolkit for Scientific Computation (PETSc) library Scalable Nonlinear Equations Solvers (SNES) [35, 36] to perform Newton iterations. In all experiments presented, we use PETSc SNES objects in Firedrake [32] and FEniCS [33] with the default settings for tolerances for the iterations.

4.1. One Dimensional Problem

The first verification we present is a spatially one dimensional Cahn-Hilliard problem in which we consider a manufactured exact solution $u(x, t)$ from [37], called the *propagating front test case*:

$$u(x, t) = \tanh \left(\frac{x - 0.5t - 0.25}{\sqrt{2\lambda}} \right). \tag{23}$$

To impose this exact solution, we apply the Cahn-Hilliard equation (2) to (23) to ascertain the corresponding right hand side and boundary conditions. We pick $D = 1$, $\lambda = 1/16$, the spatial domain $\Omega = (0, 1)$, and the final time $T = 1.0\text{s}$, i.e., $\Omega_T = (0, 1) \times (0, 1)$. This exact solution is shown in Figure 2. As the problem is one dimensional in space, the functions spaces $H(\text{div}, \Omega)$ and $H^1(\Omega)$ coincide. Hence, we use classical Lagrangian basis functions for all trial variables, which are now scalar valued.

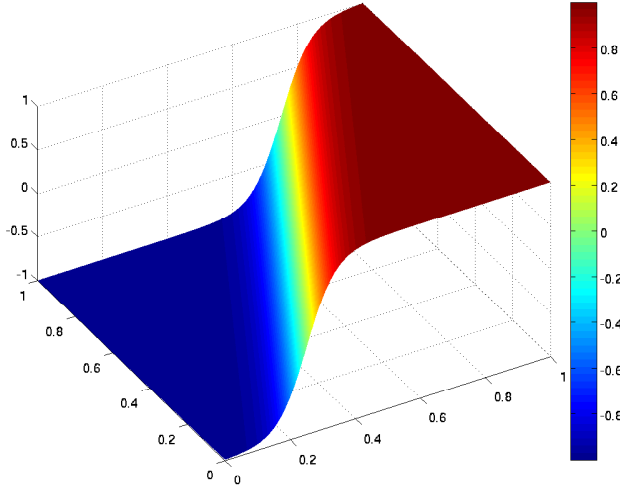


Fig. 2. Exact solution $u(x,t)$ of the propagating front problem

4.1.1. Numerical Asymptotic Convergence Study

As an initial experiment, we implement the one dimensional problem in Firedrake in which we start with a uniform space-time mesh consisting of two triangle elements to which we perform successive uniform h -refinements. For the base variable u the expected rates of convergence in classical Sobolev type norms are:

$$\begin{aligned} \|u - u^h\|_{L^2(\Omega)} &\leq Ch^p && \text{if } p < 3, \\ \|u - u^h\|_{L^2(\Omega)} &\leq Ch^{p+1} && \text{if } p \geq 3, \\ \|u - u^h\|_{H^1(\Omega)} &\leq Ch^p. \end{aligned} \tag{24}$$

The derivations of these bounds are omitted here, and we refer the interested reader to [20] for the necessary details to derive *a priori* error estimates for the AVS-FE method as well as [38] for error estimates of the Cahn-Hilliard equation. Note that for $p < 3$, the L^2 and H^1 norms of the approximation error converge at the same rate.

In Figure 3, we show the convergence history for uniform h refinements, and increasing orders of approximation, p , for $u - u^h$, $q - q^h$ showing higher rates than predicted for $p = 1$ and $p = 2$ and good agreement with the rates predicted in (24) for $p = 3$. In Figure 3(a), the rates are $h^{p+0.6}$, $h^{p+0.8}$ and h^{p+1} , for linear, quadratic and cubic polynomials, respectively, and the rates in Figure 3(b) h^p for all polynomial degrees.

4.1.2. Mesh Adaptive Refinements

Having numerically verified the convergence properties of the AVS-FE method for the Cahn-Hilliard equation let us now consider mesh-adaptive refinements. By implementing the AVS-FE method as a mixed problem (21), we establish both the approximate solutions u^h , q^h , etc. and the error representation function $(\psi^h, \phi^h, \xi^h, \eta^h)$. Hence, the restriction of this estimate to each element will be used as an error indicator:

$$\eta = \|(\psi^h, \phi^h, \xi^h, \eta^h)\|_{V(K_m)} \tag{25}$$

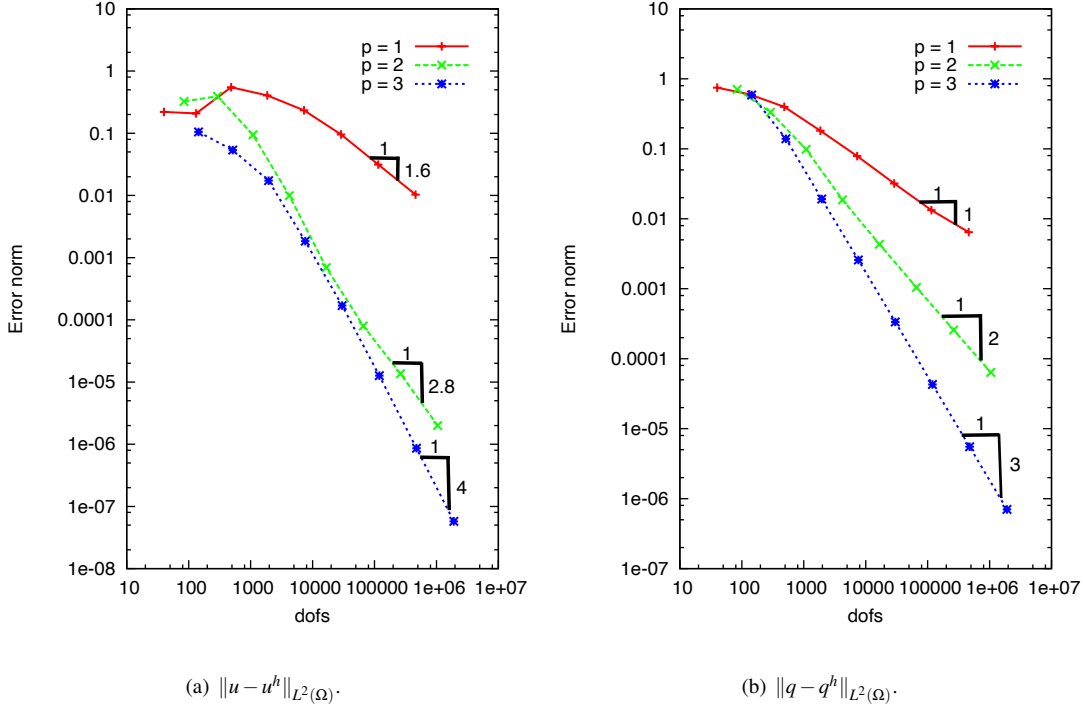


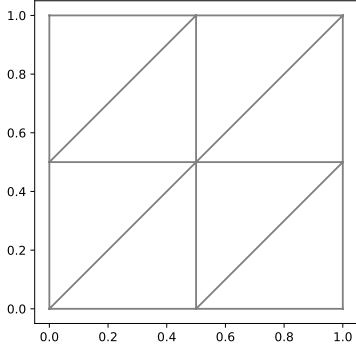
Fig. 3. Error convergence results for uniform h -refinements.

This error indicator has been successfully applied for the AVS-FE method for the linear convection-diffusion PDE and to several classes of problems of the DPG [25, 28]. The stabilized adaptive method of Calo *et al.* [39] also utilizes this type error indicator.

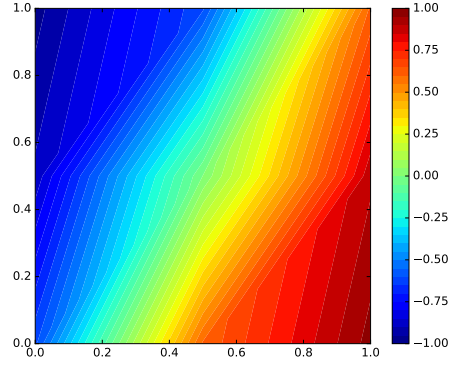
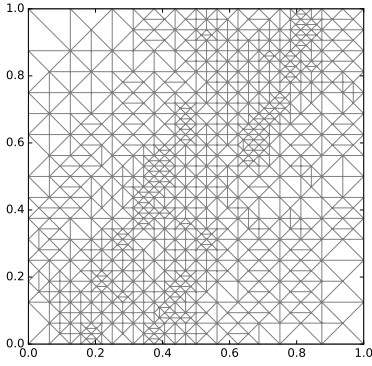
The one dimensional problem is implemented in FEniCS starting with a uniform mesh consisting of eight triangle elements to which we perform successive adaptive mesh refinements based on the error indicator η and we employ the marking strategy of [40]. All physical problem parameters are as in the preceding verification and we use quadratic polynomial approximations for all solution variables. In Figures 4, 5, and 6 we show selected meshes and corresponding solutions from the refinement process. The AVS-FE built-in error indicator performs very well as the mesh refinements are focused along the propagating front. Finally, in Figure 7 we show the convergence history of $\|u - u^h\|_{L^2(\Omega)}$ and $\|q - q^h\|_{L^2(\Omega)}$. Comparison of the convergence plots in Figure 7 and those for the uniform mesh refinement in Figure 3 show that the adaptive algorithm is capable of establishing accurate approximations at a lower cost. The advantage is that the computational efforts are focused in important regions where the solution undergoes large changes.

4.2. Two Dimensional Problem

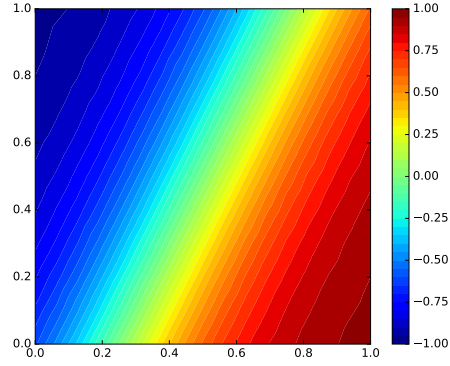
In this section we consider a two dimensional benchmark problem for the Cahn-Hilliard equation as the target physical application of mineral separation falls into this category. This commonly applied problem for the Cahn-Hilliard equation governs the evolution of two distinct phases in a medium, see, e.g., [41, 42]. The problem is chosen



(a) Mesh.

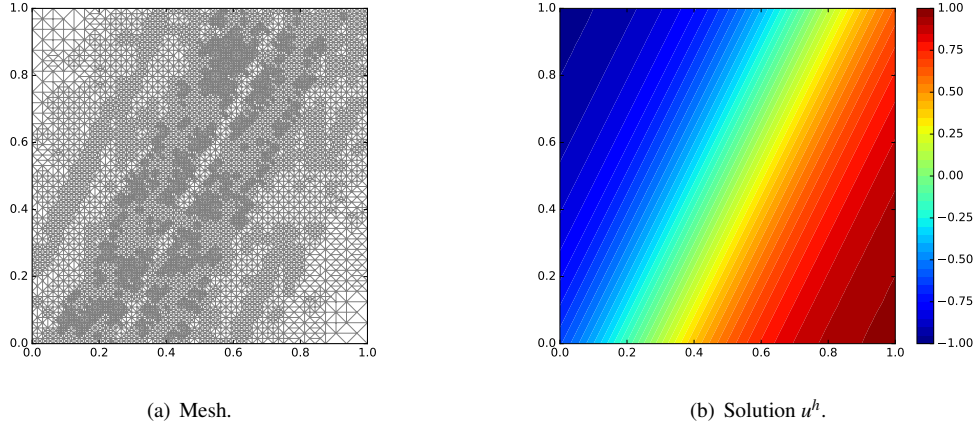
(b) Solution u^h .**Fig. 4. Initial adaptive step.**

(a) Mesh.

(b) Solution u^h .**Fig. 5. 14'th adaptive step.**

as it depicts a phase transformation and convergence towards a steady state. We consider physical properties as chosen by Brenner *et al.* [42]: $D = 1$, $\lambda = 0.01$, and the spatial domain consist of the unit square. The domain is initially occupied by two phases of material, one of which is shaped like a cross. Inside the cross, the phase is given the value $+1$ whereas it is -1 outside the cross. This initial condition is given by the piecewise constant function shown in Figure 8. Based on this initial condition, the boundary conditions are $u = -1$ and $q = 0$ on $\partial\Omega$.

To facilitate comparison with the results presented by Brenner *et al.* [42], we consider a case in which the final time $T = 0.015625s$, as the binary mixture is expected to have reached a steady state at this time. The computations are performed by employing the "extruded mesh" feature of Firedrake [32]. To this end, we consider the case in which Ω_T is discretized by 64×64 triangular elements spatially that are extruded into tetrahedrons in the time domain of width equal to half the final time. We use linear polynomials spatially and fifth order polynomials in time for all trial variables in this case. Due to the stability property of the AVS-FE method, we are able to utilize such coarse discretization in time that consists of only two elements. In Figures 9 and 10, the solution is shown at

**Fig. 6. Final adaptive step.**

$t = 0.0015625s, 0.0046875s, 0.09375s$ and $0.015625s$, respectively. The transformation of the binary phases from the initial to the steady state proceeds as expected and at the final time has reached the steady state in which the two phases are separated by a circle.

Using the AVS-FE method in both space and time makes the comparison to other FE methods for the Cahn-Hilliard equation non-trivial. In terms of accuracy, the AVS-FE method delivers comparable results to those reported in, e.g., [41, 42] based on visual inspection and comparison of the results. The consideration of computational complexity is postponed to future research efforts in which other methods are to be considered for the time discretization. For this particular problem, the total number of degrees of freedom is 2094797, while the number of degrees of freedom corresponding to the solution variables $(u^h, q^h, \mathbf{r}^h, \mathbf{t}^h)$ is 371800. The structure of the discrete problem (21) is such that the degrees of freedom corresponding to the error indicator can be condensed out through a Schur complement argument thereby drastically reducing the number of degrees of freedom of the system of linear algebraic equations.

5. Conclusions

We have presented an application of the AVS-FE method to the Cahn-Hilliard equation to establish unconditionally stable AVS-FE approximations of the nonlinear Cahn-Hilliard equation in both space and time.

The AVS-FE method results in FE approximations that converge to the exact solution at optimal rates. This was illustrated by a one dimensional experiment to which an exact solution exist in Section 4.1.1. Furthermore, the AVS-FE method comes with a built-in error estimate and the resulting error indicator has been used to successfully drive mesh adaptive refinements in both space and time. Finally, a benchmark problem from literature was implemented in which the Cahn-Hilliard problem leads to a phase transition between two binary phases in a medium. The results for this case show that the AVS-FE method is capable of delivering accurate space-time computations for spatially two dimensional problems. Focus is given here to the use of the AVS-FE method in both space and time due to its unconditional stability. Other time discretizations can also be considered, e.g., finite difference techniques or generalized α method [43–46]. For now we leave these techniques for future works that involve spatially three

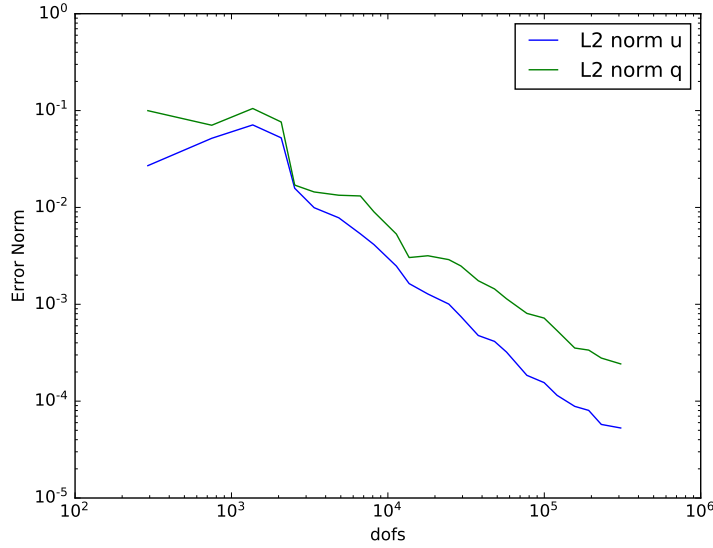


Fig. 7. Error convergence results for adaptive h -refinements for the one dimensional model problem.

dimensional problems, in which the space time approach of this paper becomes less feasible due to the need for four dimensional mesh generation.

While the computational cost of the space-time AVS-FE approach we have presented in this paper is high it has the advantage that we can solve transient BVPs using a single global solve in space and time. Additionally, the stability property of the AVS-FE enables users to start with a very coarse space-time mesh which can be adaptively refined using the built-in error indicator. Hence, our method is a viable option to classical time stepping algorithms and the entire solution process is easily amendable to parallel processing. Furthermore, a static condensation process through a Schur complement can further reduce the computational cost. While we have not been able to implement this in our current computational framework it is to be one of our foci for future research efforts.

Acknowledgements

The authors are grateful for the contributions of Professor Jon Kellar, Professor William Cross, and Mr. Bernardo Sansao of the Department of Materials and Metallurgical Engineering at the SDSM&T through fruitful discussions on mineral separation and the Cahn-Hilliard equation.

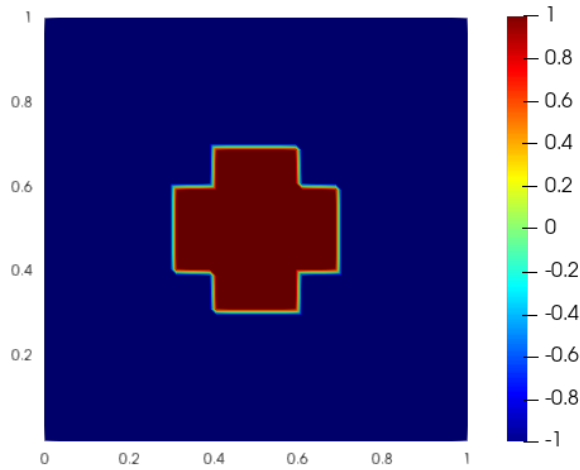


Fig. 8. Initial condition for the two dimensional model problem.

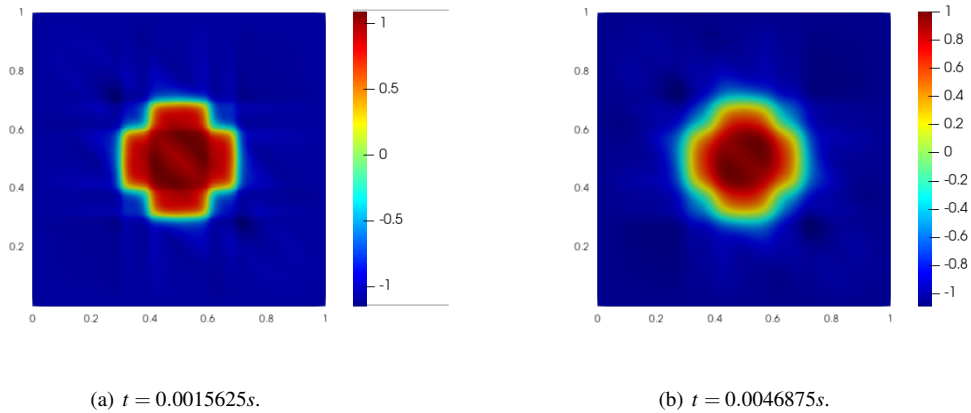


Fig. 9. AVS-FE approximation u^h of Cahn-Hilliard equation with initial condition shown in Figure 8

References

- [1] T. Wisdom, Recent developments in tailings dewatering technology, presented at the Society for Mining, Metallurgy and Exploration Annual Meeting, February 26, 2020, Phoenix, AZ.
- [2] C. M. Elliott, Z. Songmu, On the Cahn-Hilliard equation, *Archive for Rational Mechanics and Analysis* 96 (4) (1986) 339–357.
- [3] J. T. Oden, *Finite elements of nonlinear continua*, Courier Corporation, 2006.
- [4] R. Courant, K. Friedrichs, H. Lewy, Über die partiellen differenzengleichungen der mathematischen physik, *Mathematische annalen* 100 (1) (1928) 32–74.
- [5] F. Chave, D. A. Di Pietro, F. Marche, F. Pigeonneau, A hybrid high-order method for the Cahn-Hilliard problem in mixed form, *SIAM Journal on Numerical Analysis* 54 (3) (2016) 1873–1898.
- [6] S. Clavijo, A. Sarmiento, L. Espath, L. Dalcin, A. Cortes, V. M. Calo, Reactive n-species Cahn-Hilliard system: A thermodynamically-consistent model for reversible chemical reactions, *Journal of Computational and Applied Mathematics* 350 (2019) 143–154.
- [7] G. N. Wells, E. Kuhl, K. Garikipati, A discontinuous Galerkin method for the Cahn-Hilliard equation, *Journal of Computational Physics* 218 (2) (2006) 860–877.
- [8] J. W. Barrett, J. F. Blowey, H. Garcke, On fully practical finite element approximations of degenerate Cahn-Hilliard systems, *ESAIM: Mathematical Modelling and Numerical Analysis* 35 (4) (2001) 713–748.

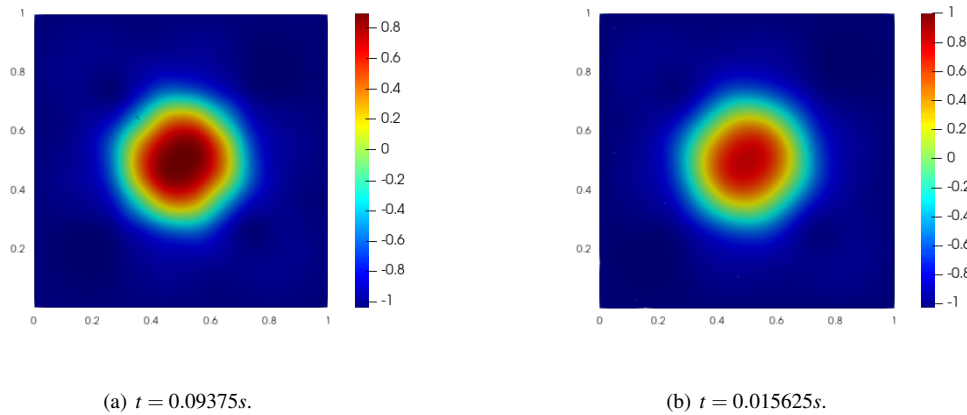


Fig. 10. AVS-FE approximation u^h of Cahn-Hilliard equation with initial condition shown in Figure 8

- [9] H. Gómez, V. M. Calo, Y. Bazilevs, T. J. Hughes, Isogeometric analysis of the Cahn-Hilliard phase-field model, *Computer methods in applied mechanics and engineering* 197 (49-50) (2008) 4333–4352.
- [10] M. Fernandino, C. Dorao, The least squares spectral element method for the Cahn-Hilliard equation, *Applied mathematical modelling* 35 (2) (2011) 797–806.
- [11] E. Dean, R. Glowinski, D. Trevas, An approximate factorization/least squares solution method for a mixed finite element approximation of the Cahn-Hilliard equation, *Japan Journal of Industrial and Applied Mathematics* 13 (3) (1996) 495.
- [12] T. J. R. Hughes, J. R. Stewart, A space-time formulation for multiscale phenomena, *Journal of Computational and Applied Mathematics* 74 (1996) 217–229.
- [13] T. J. Hughes, G. M. Hulbert, Space-time finite element methods for elastodynamics: formulations and error estimates, *Computer methods in applied mechanics and engineering* 66 (3) (1988) 339–363.
- [14] A. K. Aziz, P. Monk, Continuous finite elements in space and time for the heat equation, *Mathematics of Computation* 52 (186) (1989) 255–274.
- [15] T. E. Ellis, L. Demkowicz, J. Chan, R. D. Moser, Space-time DPG: Designing a method for massively parallel CFD, ICES report, The Institute for Computational Engineering and Sciences, The University of Texas at Austin (2014) 14–32.
- [16] T. Ellis, J. Chan, L. Demkowicz, Robust DPG methods for transient convection-diffusion, in: *Building bridges: connections and challenges in modern approaches to numerical partial differential equations*, Springer, 2016, pp. 179–203.
- [17] N. V. Roberts, L. Demkowicz, R. Moser, A discontinuous Petrov–Galerkin methodology for adaptive solutions to the incompressible navier–stokes equations, *Journal of Computational Physics* 301 (2015) 456–483.
- [18] P. B. Bochev, M. D. Gunzburger, *Least-Squares Finite Element Methods*, Vol. 166, Springer Science & Business Media, 2009.
- [19] V. M. Calo, A. Romkes, E. Valseth, Automatic Variationally Stable Analysis for FE Computations: An Introduction, *Lecture Notes in Computational Science and Engineering*, accepted, arXiv preprint arXiv:1808.01888. (2018).
- [20] E. Valseth, *Automatic Variationally Stable Analysis for Finite Element Computations*, Ph.D. thesis (2019).
- [21] L. Demkowicz, J. Gopalakrishnan, A class of discontinuous Petrov–Galerkin methods. Part I: The transport equation, *Computer Methods in Applied Mechanics and Engineering* 199 (23) (2010) 1558–1572.
- [22] C. Carstensen, P. Bringmann, F. Hellwig, P. Wriggers, Nonlinear discontinuous Petrov–Galerkin methods, *Numerische Mathematik* 139 (3) (2018) 529–561.
- [23] J. W. Cahn, J. E. Hilliard, Free energy of a nonuniform system. i. interfacial free energy, *The Journal of chemical physics* 28 (2) (1958) 258–267.
- [24] L. Demkowicz, J. Gopalakrishnan, Discontinuous Petrov–Galerkin (DPG) method (2015).
- [25] C. Carstensen, L. Demkowicz, J. Gopalakrishnan, A posteriori error control for DPG methods, *SIAM Journal on Numerical Analysis* 52 (3) (2014) 1335–1353.
- [26] L. Demkowicz, J. Gopalakrishnan, Analysis of the DPG method for the Poisson equation, *SIAM Journal on Numerical Analysis* 49 (5) (2011) 1788–1809.
- [27] L. Demkowicz, J. Gopalakrishnan, A class of discontinuous Petrov–Galerkin methods. II. Optimal test functions, *Numerical Methods for Partial Differential Equations* 27 (1) (2011) 70–105.
- [28] L. Demkowicz, J. Gopalakrishnan, A class of discontinuous Petrov–Galerkin methods. Part III: Adaptivity, *Applied numerical mathematics* 62 (4) (2012) 396–427.
- [29] L. F. Demkowicz, J. Gopalakrishnan, An overview of the discontinuous Petrov Galerkin method, in: *Recent developments in discontinuous Galerkin finite element methods for partial differential equations*, Springer, 2014, pp. 149–180.
- [30] M. Woźniak, M. Łoś, M. Paszyński, L. Demkowicz, Fast parallel integration for three dimensional discontinuous Petrov Galerkin method, *Procedia Computer Science* 101 (2016) 8–17.
- [31] N. V. Roberts, T. Bui-Thanh, L. Demkowicz, The DPG method for the Stokes problem, *Computers & Mathematics with Applications* 67 (4) (2014) 966–995.

- [32] F. Rathgeber, D. A. Ham, L. Mitchell, M. Lange, F. Luporini, A. T. McRae, G.-T. Bercea, P. H. Markall, Graham R. and Kelly, Firedrake: automating the finite element method by composing abstractions, *ACM Transactions on Mathematical Software (TOMS)* 43 (3) (2017) 24.
- [33] M. S. Alnæs, J. Blechta, J. Hake, A. Johansson, B. Kehlet, A. Logg, C. Richardson, J. Ring, M. E. Rognes, G. N. Wells, The FEnics project version 1.5, *Archive of Numerical Software* 3 (100) (2015) 9–23.
- [34] V. Girault, P.-A. Raviart, Finite element methods for Navier-Stokes equations; theory and algorithms, in: *Springer Series in Computational Mathematics*, Vol. 5, Springer-Verlag, 1986.
- [35] S. Abhyankar, J. Brown, E. M. Constantinescu, D. Ghosh, B. F. Smith, H. Zhang, Petsc/ts: A modern scalable ode/dae solver library, *arXiv preprint arXiv:1806.01437* (2018).
- [36] S. Balay, S. Abhyankar, M. F. Adams, J. Brown, P. Brune, K. Buschelman, L. Dalcin, A. Dener, V. Eijkhout, W. D. Gropp, D. Karpeyev, D. Kaushik, M. G. Knepley, D. A. May, L. C. McInnes, R. T. Mills, T. Munson, K. Rupp, P. Sanan, B. F. Smith, S. Zampini, H. Zhang, H. Zhang, PETSc users manual, Tech. Rep. ANL-95/11 - Revision 3.12, Argonne National Laboratory (2019).
URL <https://www.mcs.anl.gov/petsc>
- [37] K. G. Van Der Zee, J. Tinsley Oden, S. Prudhomme, A. Hawkins-Daarud, Goal-oriented error estimation for Cahn-Hilliard models of binary phase transition, *Numerical Methods for Partial Differential Equations* 27 (1) (2011) 160–196.
- [38] M. Kästner, P. Metsch, R. De Borst, Isogeometric analysis of the Cahn-Hilliard equation-a convergence study, *Journal of Computational Physics* 305 (2016) 360–371.
- [39] V. M. Calo, A. Ern, I. Muga, S. Rojas, An adaptive stabilized finite element method based on residual minimization, *arXiv preprint arXiv:1907.12605* (2019).
- [40] W. Dörfler, A convergent adaptive algorithm for Poisson's equation, *SIAM Journal on Numerical Analysis* 33 (3) (1996) 1106–1124.
- [41] L. Goudenège, D. Martin, G. Vial, High order finite element calculations for the Cahn-Hilliard equation, *Journal of Scientific Computing* 52 (2) (2012) 294–321.
- [42] S. C. Brenner, A. E. Diegel, L.-Y. Sung, A robust solver for a second order mixed finite element method for the Cahn-Hilliard equation, *Journal of Computational and Applied Mathematics* 364 (2020) 112322.
- [43] P. Behnoudfar, E. Valseeth, V. Calo, A. Romkes, Automatic Variationally Stable Analysis for Finite Element Computations: Transient Problems: In Preparation, To be submitted in *Computer Methods in Applied Mechanics and Engineering* (2020).
- [44] Q. Deng, P. Behnoudfar, V. M. Calo, High-order generalized- α methods, *arXiv preprint arXiv:1902.05253* (2019).
- [45] P. Behnoudfar, Q. Deng, V. M. Calo, Higher-order generalized- α methods for hyperbolic problems, *arXiv preprint arXiv:1906.06081* (2019).
- [46] J. Chung, G. Hulbert, A time integration algorithm for structural dynamics with improved numerical dissipation: the generalized- α method, *Journal of Applied Mechanics* 60 (2) (1993) 371–375.